ELSEVIER

Chemical Engineering Journal 95 (2003) 83–93

Chemical Engineering Journal

www.elsevier.com/locate/cej

Adsorption-enhanced steam-methane reforming with intraparticle-diffusion limitations☆

Guohua Xiu, Ping Li, Alirio E. Rodrigues*

Laboratory of Separation and Reaction Engineering (LSRE), Faculty of Engineering, University of Porto, Rua Dr. Roberto Frias s/n, 4200-465 Porto, Portugal

Received 11 October 2002; accepted 31 March 2003

Abstract

The adsorption-enhanced reaction (AER) process is theoretically analyzed for hydrogen production by steam-methane reforming (SMR). It uses a fixed-bed packed column of an admixture of a SMR catalyst and an adsorbent for selective removal of CO_2 from the reaction zone. A mathematical model taking into account multicomponent (six species) mass balances, overall mass balance, Ergun relation for pressure drop, energy balance for bed-volume element including the heat-transfer to the column wall, and nonlinear adsorption equilibrium isotherm coupled with three main reactions was derived to describe AER process with the intraparticle-diffusion limitations. The numerical solution of the model equations for this process was obtained by using the method of orthogonal collocation. The validity of the model prediction was checked by comparing the simulated results with experimental data from literature. The mechanism of the adsorption-enhanced SMR is studied by analysis of the profiles of the bed concentrations, temperature, velocity, pressure, and reaction and adsorption rates. The intraparticle-diffusion limitations on the adsorption-enhanced SMR are evaluated by the effectiveness factors. The effect of the operating conditions (reaction temperature, pressure and length of adsorptive reactor) on the hydrogen purity, hydrogen productivity and methane conversion is studied by numerical simulation; a high purity of hydrogen product gas (90–98%) with methane as the prime impurity and traces of CO_2 (below 400 ppm) and CO (below 30 ppm) can be produced directly from the adsorptive reactor under conditions of 450–490 °C and 222.9–891.4 kPa.

Keywords: Adsorption; Mass-transfer; Mathematical modeling; Reaction engineering; Adsorption-enhanced reaction (AER) process; Effectiveness factor

1. Introduction

Many chemical reactions are usually limited by thermodynamic equilibrium or catalyst selectivity. On the other hand, the separation step and reactant recycle requires vast amount of energy and often generates a significant amount of waste products. Therefore, it is beneficial to couple reaction and separation within one single unit, which can lead to higher or sometimes to complete conversion and purer product in a single unit by crossing the boundaries of the thermodynamic equilibrium conversion or catalyst selectivity [1–11].

The steam-methane reforming (SMR) to produce hydrogen in an adsorptive reactor is a typical example. In a conventional reactor (without adsorbent), high reaction temperature (700–1000 °C) and high pressure (about 2200 kPa) are adopted for SMR, the methane conversion obtained is about 80%, the product gas contains amounts of CO and CO_2; therefore, the ancillary processes such as water–gas shift reaction, alkali absorption and methanation are needed in order to remove CO and CO_2, respectively, from the product gas for further uses. However, in an adsorptive reactor packed with an admixture of SMR catalyst and adsorbent for selectively removing CO_2 from the reaction zone, the SMR is enhanced and the hydrogen enriched product gas with traces of CO and CO_2 can be directly produced at relatively low temperature [8,9]. Once the adsorbent is saturated with CO_2, the regeneration of the adsorbent is performed by pressure-swing adsorption in situ. For example, 88–95% H_2 with methane as the primary impurity and traces of CO_2 (less than 130 ppm) and CO (not detectable; below 50 ppm) can be produced by reaction of steam and methane in a 6 m pilot-scale adsorptive reactor at 490 °C and 180–450 kPa [12].

Characteristics of the system treated are the close interaction between multi-reaction and heat and mass-transfer mechanisms. Therefore, it is hard to identify reliably

☆ A part of this paper is presented in 17th International Symposium on Chemical Reaction Engineering, Hong Kong, China, 25–28 August 2002.

* Corresponding author. Tel.: +351-22-508-1671; fax: +351-22-508-1674.
E-mail address: arodrig@fe.up.pt (A.E. Rodrigues).

1385-8947/$ – see front matter © 2003 Elsevier Science B.V. All rights reserved.
doi:10.1016/S1385-8947(03)00116-5

Nomenclature

b_{CO_2}	Langmuir model constant for component CO_2 (Pa^{-1})
c	total molar concentration in the pellets ($mol\,m^{-3}$)
$\langle c \rangle$	volumed-average total molar concentration in the pellets ($mol\,m^{-3}$)
c_i	molar concentration in the pellets for component i ($mol\,m^{-3}$)
$\langle c_i \rangle$	volumed-average molar concentration in the pellets for component i ($mol\,m^{-3}$)
C	total molar concentration in the bulk phase ($mol\,m^{-3}$)
C_i	molar concentration of gas-phase component i ($mol\,m^{-3}$)
$C_{p,g}$	gas-phase heat capacity ($J\,mol^{-1}\,K^{-1}$)
$C_{p,s}$	solid-phase heat capacity ($J\,kg^{-1}\,K^{-1}$)
$C_{v,g}$	heat capacity of gas-phase at constant volume ($J\,mol^{-1}\,K^{-1}$)
d_p	particle diameter (m)
D_p	Fickian pore diffusivity ($m^2\,s^{-1}$)
D_M	molecular diffusivity ($m^2\,s^{-1}$)
D_L	axial dispersion coefficient ($m^2\,s^{-1}$)
$-\Delta H_{ad,i}$	adsorption heat of component i (on the adsorbent surface) ($J\,mol^{-1}$)
$\Delta H_{R,i}$	reaction heat of reaction i ($J\,mol^{-1}$)
k_{fi}	mass-transfer coefficient (s^{-1})
k_j	rate constant of reaction j, j = I, II ($mol\,Pa^{0.5}\,kg^{-1}$ catalyst s^{-1}), j = III ($mol\,kg^{-1}$ catalyst s^{-1})
k_z	effective thermal conductivity ($J\,m^{-1}\,s^{-1}\,K^{-1}$)
K_j	equilibrium constant, j = I, II (Pa^2), j = III
K_D	Ergun equation coefficient ($N\,s\,m^{-4}$)
K_V	Ergun equation coefficient ($N\,s^2\,m^{-5}$)
L	reactor length (m)
m_{CO_2}	Langmuir model constant for component CO_2 ($mol\,kg^{-1}$)
M	molecular weight ($kg\,mol^{-1}$)
p	local total pressure in the catalyst pellet (Pa)
p_i	partial pressure of gas-phase component i in the catalyst pellet (Pa)
P	local total pressure in the bulk phase (Pa)
P_i	partial pressure of gas-phase component i (Pa)
P_H	high pressure (Pa)
q_i	solid-phase concentration for component i ($mol\,kg^{-1}$)
$\bar{q}_i$	volumed-average solid-phase concentration for component i over an adsorbent particle ($mol\,kg^{-1}$)
r_p	radius of the pellets (m)
R_0	inner radius of the reactor (m)
R_j	reaction rate defined by Eq. (1) ($mol\,kg^{-1}$ catalyst s^{-1})
$\Re_i$	formation or consumption rate of component i ($mol\,kg^{-1}$ catalyst s^{-1})
t	time (s)
T	temperature in bulk gas-phase (K)
T_f	feed gas temperature (K)
T_w	wall temperature (K)
u	superficial velocity ($m\,s^{-1}$)
u_f	feed gas superficial velocity ($m\,s^{-1}$)
U	overall bed-wall heat-transfer coefficient ($J\,m^{-2}\,K^{-1}$)
x_i	gas-phase mole fraction of component i in pellets
y_{fi}	gas-phase mole fraction of component i in the feed
y_i	gas-phase mole fraction of component i
z	axial coordinate in bed (m)

Greek letters

α	mass ratio of adsorbent and catalyst in the packed-bed
ε	porosity
ε_b	bed porosity
ε_t	total bed porosity
η_j	catalyst effectiveness factor
μ	viscosity of fluid ($kg\,m^{-1}\,s$)
ρ_{ad}	mass of adsorbent in the bed volume ($kg\,m^{-3}$)
ρ_b	buck packing density ($kg\,m^{-3}$)
ρ_{cat}	mass of catalyst in the bed volume ($kg\,m^{-3}$)
ρ_g	gas-phase density ($kg\,m^{-3}$)
$\rho_{p,ad}$	density of the adsorbent ($kg\,m^{-3}$)
$\rho_{p,cat}$	density of the catalyst ($kg\,m^{-3}$)
τ	tortuosity factor of the catalyst

feasibility or to establish independently the values of individual model parameters experimentally. The most effective way of proceeding is thus through deliberate experimentation supported by physically realistic simulation. Ding and Alpay [9] investigated the adsorption-enhanced SMR theoretically and experimentally. Later, Xiu et al. [10,11] extended the theoretical analysis to the cyclic operation. In the above works, the diffusion process in the adsorbent is described by the LDF model, and the effectiveness factors for SMR process were taken as constant. However, due to commercial large size of catalyst and adsorbent pellets used in practice, the above-simplified treatments may cause some deviation from the real situation for the adsorptive reactor. Therefore, it is necessary to develop a mathematical model to check the effects of the intraparticle-diffusion limitations on the AER process.

Many publications on the subject of catalytic reactions have mentioned the intraparticle-diffusion effects using the dusty-gas model on the steady state [13–18]. However, there is not a complete description of kinetics that includes proper modeling of the intraparticle-diffusion limitations for the AER process; the adsorption-enhanced SMR process is an unsteady and complicated one in nature. In view of the complexity of the adsorptive reactor described above the problems can only be solved with the aid of advanced numerical algorithms.

In this paper, the AER process is analyzed for hydrogen production by SMR. Compared with the previous work of Xiu et al. [10,11], the objective of this work is to investigate the intraparticle-diffusion limitations on adsorption-enhanced SMR. A model taking into account multicomponent (six species) mass balances, overall mass balance, Ergun relation [19] for pressure drop, energy balance for bed-volume element including the heat-transfer to the column wall, and nonlinear adsorption equilibrium isotherm coupled with three main reactions was derived to describe the AER process. The Fickian diffusion model was adopted to evaluate the effectiveness factors for the multi-reaction system. For simplification, only one component (i.e. CO_2) was assumed to be adsorbed. Numerical solution of model equations for this process was obtained by using the method of orthogonal collocation.

2. Theoretical model

2.1. Reaction kinetics of steam-methane reforming (SMR)

The SMR can be described by the following main three chemical reactions:

$$\begin{cases} CH_4 + H_2O \Leftrightarrow CO + 3H_2, \quad \Delta H_{298} = 206.2\,\text{kJ mol}^{-1} & \text{(I)} \\ CH_4 + 2H_2O \Leftrightarrow CO_2 + 4H_2, \quad \Delta H_{298} = 164.9\,\text{kJ mol}^{-1} & \text{(II)} \\ CO + H_2O \Leftrightarrow CO_2 + H_2, \quad \Delta H_{298} = -41.1\,\text{kJ mol}^{-1} & \text{(III)} \end{cases} \quad (1)$$

The reaction kinetic model can be summarized as [20]

$$R_I = \frac{1}{(\text{DEN})^2}\frac{k_I}{p_{H_2}^{2.5}}\left(p_{CH_4}p_{H_2O} - \frac{p_{H_2}^3 p_{CO}}{K_I}\right) \quad (1a)$$

$$R_{II} = \frac{1}{(\text{DEN})^2}\frac{k_{II}}{p_{H_2}^{3.5}}\left(p_{CH_4}p_{H_2O}^2 - \frac{p_{H_2}^4 p_{CO_2}}{K_{II}}\right) \quad (1b)$$

$$R_{III} = \frac{1}{(\text{DEN})^2}\frac{k_{III}}{p_{H_2}}\left(p_{CO}p_{H_2O} - \frac{p_{H_2}p_{CO_2}}{K_{III}}\right) \quad (1c)$$

where $\text{DEN} = 1 + K_{CO}p_{CO} + K_{H_2}p_{H_2} + K_{CH_4}p_{CH_4} + K_{H_2O}p_{H_2O}/p_{H_2}$, in which $p_i = x_{i,\text{cat}}p$ ($i = H_2O$, CH_4, H_2, CO_2, CO, p and $x_{i,\text{cat}}$ are the total pressure and the gas-phase mole fraction of component i in the catalyst pellet, respectively), k_I, k_{II}, and k_{III} are the rate constants, K_I, K_{II}, and K_{III} are the equilibrium data [21]. The expressions of these parameters are listed in Table 1.

Table 1
Parameters used in Eq. (1) [20,21]

$$K_I = \frac{1}{\exp(0.2513Z^4 - 0.3665Z^3 - 0.58101Z^2 + 27.1337Z - 3.2770)}\ \text{atm}^{2\,[a]}$$

$$K_{II} = K_I K_{III}$$

$$K_{III} = \exp(-0.29353Z^3 + 0.63508Z^2 + 4.1778Z + 0.31688)^{[a]}, \quad \text{where } Z = \frac{1000}{T} - 1$$

$$k_1 = 1.842 \times 10^{-4}\exp\left[-\frac{240\,100}{R}\left(\frac{1}{T} - \frac{1}{648}\right)\right]\ \text{kmol bar}^{0.5}\,\text{kg}^{-1}\,\text{catalyst h}^{-1}$$

$$k_2 = 2.193 \times 10^{-5}\exp\left[-\frac{243\,900}{R}\left(\frac{1}{T} - \frac{1}{648}\right)\right]\ \text{kmol bar}^{0.5}\,\text{kg}^{-1}\,\text{catalyst h}^{-1}$$

$$k_3 = 7.558\exp\left[-\frac{67\,130}{R}\left(\frac{1}{T} - \frac{1}{648}\right)\right]\ \text{kmol kg}^{-1}\,\text{catalyst h}^{-1}\,\text{bar}^{-1}$$

$$K_{CH_4} = 0.179\exp\left[\frac{38\,280}{R}\left(\frac{1}{T} - \frac{1}{823}\right)\right]\ \text{bar}^{-1}$$

$$K_{H_2O} = 0.4152\exp\left[-\frac{88\,680}{R}\left(\frac{1}{T} - \frac{1}{823}\right)\right]$$

$$K_{CO} = 40.91\exp\left[\frac{70\,650}{R}\left(\frac{1}{T} - \frac{1}{648}\right)\right]\ \text{bar}^{-1}$$

$$K_{H_2} = 0.0296\exp\left[\frac{82\,900}{R}\left(\frac{1}{T} - \frac{1}{648}\right)\right]\ \text{bar}^{-1}$$

[a] Taken from Twigg [21]. The data of Xu and Froment [20] are as follows: $K_I = 4.707 \times 10^{12}\exp(-224\,000/RT)\,\text{bar}^2$, $K_{III} = 1.142 \times 10^{-2}\exp(37\,300/RT)$ (for $T = 948$ K).

2.2. Momentum, mass and energy balance equation for AER process

The theoretical model adopted for the AER process is a non-isothermal, non-adiabatic, and non-isobaric operation, developed to describe both SMR and adsorption-enhanced SMR processes. The model assumptions adopted are summarized as follows [9–11,22].

(1) The flow is represented by an axial-dispersed plug-flow model. Mass dispersion in the axial direction is considered, with negligible radial gradients. The axial dispersion coefficient was estimated from the correlation of Edwards and Richardson [23], as shown in Table 2. Change of flow due to reactions and adsorption, as determined by the overall material balance, is taken into account. The gas is assumed to be an ideal gas.
(2) Pressure distribution in the packed-bed adsorptive reactor was described by Ergun equation [19].
(3) The system is non-isothermal. The column wall and the feed stream are maintained at the same constant temperature. The heat-transfer resistance between the gas and pellet phases is neglected. Thermal dispersion in the axial direction is considered, with negligible radial gradients. Axial thermal conductivity is estimated using the empirical correlation given by Yagi et al. [24], as reproduced in Table 2. For a packed-bed with spherical particles, the wall-bed heat-transfer coefficient, U, is given by De Wash and Froment [25] and Li and Finlayson

Table 2
Parameters for the governing equations

Semi-empirical relationships for K_D and K_V [19]

$K_D = \frac{150\mu(1-\varepsilon_b)^2}{d_p^2\varepsilon_b^3}$ (N s m^{-4}), $K_V = \frac{1.75(1-\varepsilon_b)}{d_p\varepsilon_b^3}\frac{PM}{RT}$ (N s^2 m^{-5}), in which $M \approx 0.018$ kg mol^{-1}

Axial dispersion coefficient D_L [23]

$D_L = 0.73D_M + \frac{0.5ud_p}{1+9.49D_M/(ud_p)}$ (m^2 s^{-1}), in which $D_M = 1.6\times10^{-5}$ m^2 s^{-1} for P_H and T_f, and $D_M = 5.6\times10^{-5}$ m^2 s^{-1} for P_L and T_f [30]

Langmuir isotherm [9]

$q^*_{CO_2} = \frac{m_{CO_2}b_{CO_2}p_{CO_2}}{1+b_{CO_2}p_{CO_2}}$, where $m_{CO_2} = 0.65$ mol kg^{-1} and $b_{CO_2} = 2.36\times10^{-4}\exp\left[\frac{17\,000}{R}\left(\frac{1}{T}-\frac{1}{673}\right)\right]$ Pa^{-1}

Mass-transfer coefficient [27]

$\frac{k_f d_p}{D_M} = 2.0 + 1.1Sc^{1/3}Re_p^{0.6}$ $(3 < Re_p < 10^4)$, where $Sc = \frac{\mu}{\rho_g D_M}$, $Re_p = \frac{\rho_g u\varepsilon_t d_p}{\mu}$

Bed effective conductivity k_z [22,24]

$\frac{k_z}{k_g} = \frac{k_z^0}{k_g} + 0.75(Pr)(Re_p)$, where $\frac{k_z^0}{k_g} = \varepsilon_t + \frac{1-\varepsilon_t}{0.139\varepsilon_t - 0.0339 + 2/3(k_g/k_p)}$,

$Pr = \frac{C_{p,g}\mu}{k_g}$, in which $k_p = 1\times10^{-2}$ J cm^{-1} s^{-1} K^{-1} and $k_g = 2.5\times10^{-4}$ J cm^{-1} s^{-1} K^{-1} (Eucken formula in Bird et al. [32])

Wall-bed heat-transfer coefficient, U [26]

$\frac{2UR_0}{k_g} = 2.03Re_p^{0.8}\exp\left(-\frac{3d_p}{R_0}\right)$ $\left(Re_p = 20-7600, \frac{d_p}{2R_0} = 0.05-0.3\right)$, and $U = 6.15\frac{k_z^0}{2R_0}$ as $Re_p \to 0$ [25]

[26]. The gas-phase and the catalyst/adsorbent pellet are assumed to be in local thermal equilibrium at all times.

(4) There exist five components (CH_4, H_2, CO_2, CO, and H_2O) in an inert carrier (N_2). The Langmuir model is adopted to describe the adsorption equilibrium for component CO_2 on the adsorbent; for the parameters of Langmuir isothermal (see Table 2).

(5) Perfect mixing of the catalyst and adsorbent pellets, and negligible catalyst deactivation.

From the above assumptions, we can derive the following governing equations and the corresponding initial and boundary conditions.

According to Eq. (1), the formation or consumption rate of component i, $\Re_i$, was calculated by

$$\Re_i = \sum_{j=\mathrm{I}}^{\mathrm{III}} v_{ij}R_j \quad (i = 1\text{–}6\ \text{component},\ j = \mathrm{I}\text{–}\mathrm{III}) \tag{2}$$

where v_{ij} is the stoichiometric coefficient of component i. If i refers to a reactant, v_{ij} is negative, and for a product v_{ij} is positive.

The overall mass balance equation in the adsorptive reactor is

$$\frac{\partial(\varepsilon_b C + \rho_{ad}\bar{q}_{CO_2})}{\partial t} + \frac{\partial(uC)}{\partial z} + (1-\varepsilon_b)\frac{\partial\langle c\rangle}{\partial t} - \rho_{cat}\sum_{i=1}^{6}\sum_{j=\mathrm{I}}^{\mathrm{III}} v_{ij}\eta_j R_j = 0 \tag{3}$$

where C is the total molar concentration in the bulk phase, u the superficial velocity, ρ_{ad} and ρ_{cat} the bulk densities of the adsorbent and the catalyst, respectively, ε_b the bed porosity, t the time, z the axial coordinate in the packed-bed, and η_j is the catalyst effectiveness factor. ρ_{ad} and ρ_{cat} are related with the bulk packing density ρ_b by $\rho_{ad} = \alpha\rho_b/(1+\alpha)$ and $\rho_{cat} = \rho_b/(1+\alpha)$, where α is the mass ratio of adsorbent and catalyst in the packed-bed.

The volumed-average concentration of c in pellets, $\langle c\rangle$, in Eq. (3) is defined as

$$\langle c\rangle = \frac{\varepsilon_{cat}\bar{c}_{cat} + \alpha\varepsilon_{ad}\bar{c}_{ad}}{1+\alpha} \tag{3a}$$

where ε_{cat} and ε_{ad} are the porosities of the catalyst and the adsorbent, and $\bar{c}_{cat}$ and $\bar{c}_{ad}$ are the volumed-average concentrations over the catalyst and the adsorbent pellets which are calculated from the corresponding local values of c_{cat} and c_{ad}, respectively.

For component i, the mass balance for the packed-bed reactor is

$$\frac{\partial(\varepsilon_b C_i + \rho_{ad}\bar{q}_i)}{\partial t} + \frac{\partial(uC_i)}{\partial z} + (1-\varepsilon_b)\frac{\partial\langle c_i\rangle}{\partial t} - \rho_{cat}\sum_{j=\mathrm{I}}^{\mathrm{III}} v_{ij}\eta_j R_j = \varepsilon_b\frac{\partial}{\partial z}\left(D_L C\frac{\partial y_i}{\partial z}\right) \tag{4}$$

where $C_i = y_i C$, y_i is the gas-phase mole fraction of component i in the bulk phase, and D_L is the axial dispersion coefficient, and

$$\langle c_i\rangle = \frac{\varepsilon_{cat}x_{i,cat}\bar{c}_{cat} + \alpha\varepsilon_{ad}x_{i,ad}\bar{c}_{ad}}{1+\alpha} \tag{4a}$$

in which $x_{i,ad}$ is the gas-phase mole fraction of component i in the adsorbent pellet.

The pressure distribution in the packed-bed reactor was described by the Ergun equation [19]

$$\frac{\partial P}{\partial z} = -K_D u - K_V u^2 \tag{5}$$

where P is the local pressure at z the axial coordinate in the bulk phase, K_D and K_V are parameters corresponding to the viscous and kinetic pressure loss terms.

The energy balance for the bed-volume element including the heat-transfer to the column wall is

$$(\varepsilon_t C C_{v,g} + \rho_b C_{p,s})\frac{\partial T}{\partial t} + C C_{p,g} u \frac{\partial T}{\partial z} - \rho_{ad}\sum_{i=1}^{6}\left(-\Delta H_{ad,i}\frac{\partial \bar{q}_i}{\partial t}\right) - \frac{2U}{R_0}(T_w - T) - \rho_{cat}\sum_{i=1}^{6}\sum_{j=I}^{III} v_{ij}\eta_j R_j \Delta H_{R,j} = \frac{\partial}{\partial z}\left(k_z \frac{\partial T}{\partial z}\right) \tag{6}$$

where $C_{p,g}$ and $C_{p,s}$ are the gas- and solid-phase heat capacity, respectively, $C_{v,g}$ the heat capacity of gas-phase at constant volume, k_z the effective thermal conductivity, $-\Delta H_{ad,i}$ the adsorption heat of component i (i.e. CO_2), $\Delta H_{R,j}$ the reaction heat of reaction j, ε_t the total porosity of the packed-bed, U the overall bed-wall heat-transfer coefficient, and R_0 is the inner radius of the reactor.

The initial and boundary conditions of Eqs. (2)–(6) are

$$T = T_f, u = 0, q_i = 0, y_{H_2} = 1, y_i = 0, P_{H_2} = P_H, P_i = 0 \quad \text{at } t = 0 \ (i = CO, CO_2, H_2O, CH_4, \text{and } N_2) \tag{7a}$$

$$\left(\frac{\partial y_i}{\partial z}\right)_{z=0} = -\frac{u_f(y_{fi} - y_i)}{\varepsilon_b D_L}, \qquad \left(\frac{\partial y_i}{\partial z}\right)_{z=L} = 0 \tag{7b}$$

$$(u)_{z=0} = u_f, \qquad \left(\frac{\partial u}{\partial z}\right)_{z=L} = 0 \tag{7c}$$

$$(P)_{z=0} = P_H, \qquad \left(\frac{\partial P}{\partial z}\right)_{z=L} = 0 \tag{7d}$$

$$\left(\frac{\partial T}{\partial z}\right)_{z=0} = -\frac{u_f C C_{p,g}(T_f - T)}{k_z}, \qquad \left(\frac{\partial T}{\partial z}\right)_{z=L} = 0 \tag{7e}$$

The values of $\bar{q}_i$, $\langle c\rangle$, $\langle c_i\rangle$, and η_j in the above equations are calculated as follows.

(1) For simplification, we assumed that the components H_2, CH_4, H_2O, CO, and N_2 are inert for the adsorbent, i.e. $\bar{q}_i = 0$ unless for $i = CO_2$, the Fickian diffusion model is adopted to describe the mass-transfer of CO_2 to the adsorbent

$$\varepsilon_{ad}\frac{\partial c_{CO_2}}{\partial t} + (1 - \varepsilon_{ad})\rho_{p,ad}\frac{\partial q_{CO_2}}{\partial t} = \frac{1}{r^2}\frac{\partial}{\partial r}\left(D_{p,CO_2} r^2 \frac{\partial c_{CO_2}}{\partial r}\right) \tag{8}$$

where $\rho_{p,ad}$ is the density of the adsorbent and r is the radial coordinate of the pellet.

The initial and boundary conditions of Eq. (8) are

$$c_{CO_2} = 0, \qquad q_{CO_2} = 0 \quad \text{at } t = 0 \tag{9a}$$

$$\left(\frac{\partial c_{CO_2}}{\partial r}\right)_{r=0} = 0 \tag{9b}$$

$$D_{p,CO_2}\left(\frac{\partial c_{CO_2}}{\partial r}\right)_{r=r_p} = k_{f,CO_2}[C_{CO_2} - (c_{CO_2})_{r=r_p}] \tag{9c}$$

where k_{f,CO_2} is the external film mass-transfer coefficient [27], q_{CO_2} the equilibrium solid-phase concentration obeys the Langmuir isotherm [28], and r_p is radius of the pellet.

By solving Eqs. (8) and (9), $\partial \bar{q}_{CO_2}/\partial t$ is then calculated by

$$\frac{\partial \bar{q}_{CO_2}}{\partial t} = \frac{3}{r_p^3}\int_0^{r_p}\frac{\partial q_{CO_2}}{\partial t} r^2 \, dr \tag{10}$$

and we assumed that $x_{i,ad}\bar{c}_{ad} = y_i C$ for all species except CO_2 in the adsorbent pellets.

(2) Due to lacking of the experimental data for the diffusion coefficient matrix, we take Fickian law to replace the generalized Fickian formulation. For multicomponent diffusion and reaction in the catalyst pellet, we have [29]

$$\varepsilon_{cat} c_{cat}\frac{\partial x_{i,cat}}{\partial t} = c_{cat} D_{p,i}\left(\frac{\partial^2 x_{i,cat}}{\partial r^2} + \frac{2}{r}\frac{\partial x_{i,cat}}{\partial r}\right) + \rho_{p,cat}\Re_i \tag{11}$$

where $\rho_{p,cat}$ is the density of the catalyst.

The initial and boundary conditions of Eq. (11) are

$$x_{i,cat} = 0, \qquad c = 0 \quad \text{at } t = 0 \tag{12a}$$

$$\left(\frac{\partial x_{i,cat}}{\partial r}\right)_{r=0} = 0 \tag{12b}$$

$$D_{p,i}\left(\frac{\partial x_{i,cat}}{\partial r}\right)_{r=r_p} = k_{fi}[y_i - (x_{i,cat})_{r=r_p}] \tag{12c}$$

When the rate of the reaction is large in comparison with the rate of diffusion, the reaction is said to be limited by diffusion. The effectiveness factor is used as a measure of diffusional resistances and for the jth reaction, it can be defined as

$$\eta_j = \frac{(3/r_p^3)\int_0^{r_p} r^2 R_j \, dr}{(R_j)_{r=r_p}} \tag{13}$$

In the above equations, the effective diffusion coefficient of the ith component for the multicomponent system, $D_{p,i}$, is defined as

$$D_{p,i} = \frac{\varepsilon_{cat} D_{M,i}}{\tau} \tag{14a}$$

Several methods for estimating $D_{M,i}$ have been proposed. The following simple weighted-averaging method based on mole composition was used in this study [30,31]

$$D_{M,i} = \frac{\sum_{k=1,k\neq i}^{n} x_k D_{ki}}{\sum_{k=1,k\neq i}^{n} x_k} \tag{14b}$$

in which

$$D_{ki} = \frac{10^{-3}T^{1.75}}{\sqrt{p[(\sum v)_k^{1/3} + (\sum v)_i^{1/3}]^2}} \frac{M_k + M_i}{M_k M_i} \tag{14c}$$

in which p is measured in atmospheres and T in Kelvin, τ the tortuosity factor of the catalyst pellet, D_M the binary molecular diffusivity, $\sum v$ the sum of atomic diffusion volumes, and M is the molecular weight.

The above equations Eqs. (2)–(14) were solved by the orthogonal collocation method [10,11]. At all collocation points, Eqs. (3) and (5) are discretized into a set of linear algebraic equations that are solved numerically by Gauss method in order to obtain the velocity and pressure distributions along the reactor. Eqs. (4) and (6) along with Eqs. (8) and (11) are discretized into a set of ordinary differential equations with initial values which are integrated in the time domain using Gear's stiff variable step integration routine in order to obtain the effectiveness factor, effluent mole fraction and temperature histories, and the mole fraction profiles within the catalyst pellets.

3. Results and discussion

The adsorptive reactor with 25 mm diameter is packed with the mixture of catalyst and adsorbent (ρ_{ad} = 466.6 kg m^{-3}, and ρ_{cat} = 233.3 kg m^{-3}), the mean pellet diameter is 3.0 mm, the density is ρ_p = 1550 kg m^{-3} for both catalyst and adsorbent pellets, the pellet porosity is 0.5, the tortuosity factor in the pellet is set 8.0, and the bed porosity is 0.47. The adsorption isotherm is selected from Ding and Alpay [28]. A feed gas mixture of $H_2O/CH_4 = 6$ (molar ratio) with traces of N_2 (about 0.001) passes through this adsorptive reactor with 0.05 m s^{-1} feed velocity under the conditions of P_H = 445.7 kPa and $T_f = T_w$ = 450 °C. The effluent mole fractions with time are shown in Fig. 1, where the length of the reactor is selected as 2 and 4 m, respectively.

It can be seen that the whole reaction region can be divided into three zones according to the adsorption behavior of CO_2 [10,11]: (1) the AER zone, where the effluent mole fraction of CO_2 is lower, adsorption enhances the conversion of methane, and the effluent mole fraction of hydrogen at the exit is higher; (2) the breakthrough zone of CO_2, where the effluent mole fraction of CO_2 increases quickly with time, the adsorbent is nearly saturated by CO_2, the enhancement is not evident, and the purity of hydrogen at the effluent gas drops rapidly; and (3) the equilibrium state zone, where the adsorbent is saturated almost entirely by

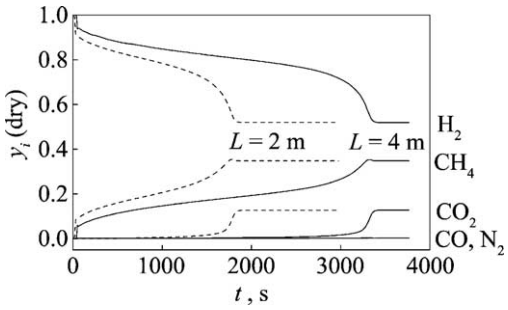

Fig. 1. Effluent mole fraction profiles at the exit of adsorptive reactor for P_H = 445.7 kPa, $T_f = T_w$ = 450 °C, u_f = 0.05 m s^{-1}, molar ratio of $H_2O/CH_4 = 6$.

CO_2 throughout the bed, the operation mode is the same as the conventional one; the SMR reaches the steady state. In the AER zone, the adsorbent selectively removes CO_2 and enhances the SMR, so higher purity hydrogen product gas with traces of CO and CO_2 can be produced. For example, if the length of adsorptive reactor is 4 m and the reaction time is controlled at t_1 = 460 s, over 92.8% average purity hydrogen with traces of CO (30 ppm) and CO_2 (383 ppm) can be directly produced; but for a conventional reactor, only 54% purity hydrogen can be obtained with amounts of CO (0.34%) and CO_2 (12.8%) due to the thermodynamic limits. The corresponding average conversion of methane is up to 73.4% for 4 m long adsorptive reactor when the reaction time is controlled at t_1 = 460 s as shown in Fig. 2, while for one conventional reactor, high temperature (about 650 °C) is needed to reach the same conversion.

Here, the conversion of methane X_{CH_4}, the average purity of hydrogen (dry basis) y_{H_2} (ave), y_i (dry basis), and the average mole of H_2 product per gram of solid are, respectively, defined as [10,11]

$$X_{CH_4} = \frac{\text{feed of CH}_4\ (\text{mol s}^{-1}) - \text{effluent of CH}_4\ (\text{mol s}^{-1})}{\text{feed of CH}_4\ (\text{mol s}^{-1})} = 1 - \left(\frac{RT_f}{u_f P_H y_{CH_4}}\right)_{\text{feed}} \left(\frac{uPy_{CH_4}}{RT}\right)_{\text{outlet}} \tag{15a}$$

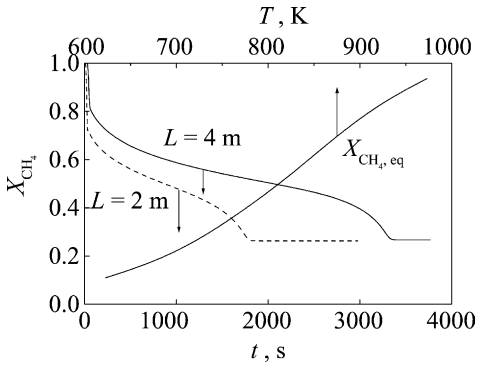

Fig. 2. Methane conversion X_{CH_4} with time and temperature for P_H = 445.7 kPa, $T_f = T_w$ = 450 °C, u_f = 0.05 m s^{-1}, molar ratio of $H_2O/CH_4 = 6$.

$$y_{H_2}\ (\text{ave}) = \frac{1}{\int_0^{t_1}((Pu(1-y_{H_2O}))/RT)_{\text{outlet}}} \times \int_0^{t_1}\left(\frac{Puy_{H_2}}{RT}\right)_{\text{outlet}} \mathrm{d}t \quad (15b)$$

$$y_i\ (\text{dry basis}) = \frac{y_i}{1-y_{H_2O}} \quad (15c)$$

$$\text{mole } H_2\ g^{-1}\ \text{solid} = \frac{1}{AL\rho_b}\int_0^{t_1}\left(\frac{Puy_{H_2}}{RT}\right)_{\text{outlet}} A\,\mathrm{d}t \quad (15d)$$

where A is the cross-sectional area of the reactor.

Figs. 3 and 4 illustrate the distribution profiles of reaction temperature (Fig. 3a), velocity (Fig. 3b), pressure (Fig. 3c) and the mole fraction distributions of CH_4 (Fig. 4a), H_2O (Fig. 4b), H_2 (Fig. 4c), CO_2 (Fig. 4d), and CO (Fig. 4e) along a 2 m long adsorptive reactor with $t = 100$, 300, 700, 1200, and 1900 s, respectively. The reaction temperature, velocity, pressure and mole fractions of reactants and products all change with time in the AER zone.

As the adsorbent is being saturated with CO_2 initially at the inlet part of the adsorptive reactor, the evident AER zone moves toward to the outlet with time, where a drop peak of the reaction temperature is observed due to the evident adsorption-enhanced SMR (reactions (I) and (II)), as shown in Fig. 3a, which results in the drop of the velocity, as shown in Fig. 3b. Due to low feed velocity being adopted, the pressure drop along the adsorptive reactor is very small (about 0.16 kPa) for 3 mm diameter pellets of catalyst and adsorbent, as shown in Fig. 3c.

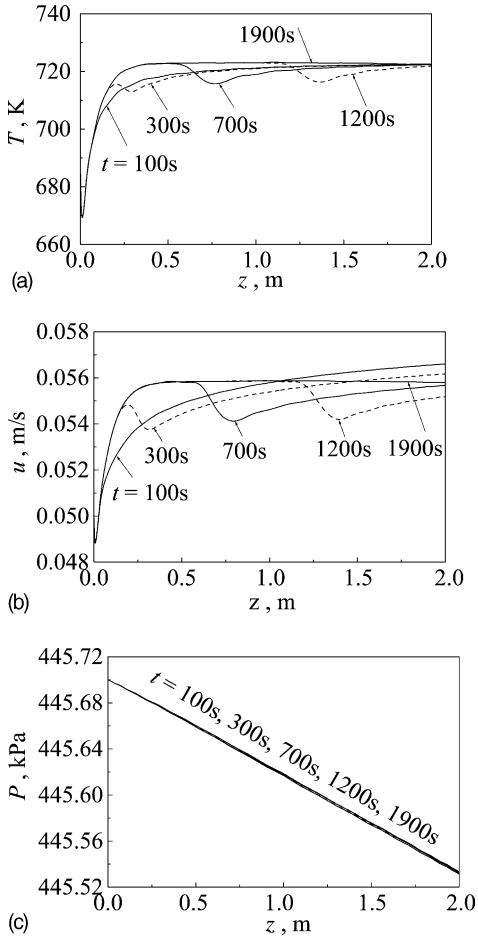

Fig. 3. Temperature (a); velocity (b); pressure (c) profiles with time in 2 m adsorptive reactor. Operation conditions are the same as those in Fig. 1.

With the adsorbent gradually saturated with CO_2, the performance of the adsorption-enhanced SMR becomes weak, results in the decrease of the methane conversion. In turn, the effluent mole fractions of remaining reactants CH_4 (Fig. 4a) and H_2O (Fig. 4b) increase and the effluent mole fraction of H_2 (Fig. 4c) decreases with time; the mole fractions of by-products CO_2 (Fig. 4d) and CO (Fig. 4e) increase with time in the effluent product gas. Once the adsorbent is entirely saturated with CO_2 throughout the bed, the performance of the AER will lost, the function of the adsorptive reactor will degrade as the conventional one. In addition, compared with Fig. 4d and e, it is found that the removal of CO_2 by adsorption also effectively suppresses the formation of the by-product CO (reaction (III)); therefore, CO concentration in the effluent gas is low. Usually, the CO concentration in the product gas is strictly controlled, for example, if the product gas is used in the fuel cell, the CO concentration should be below 30 ppm.

The mechanism of the adsorption-enhanced SMR is studied further by comparison the distributions of reaction rates (at the surface of the catalyst pellet; Fig. 5) and the adsorption rate (q_{av,CO_2} is volumed-average; Fig. 6) in a 2 m long adsorptive reactor at the AER zone. At the inlet part of the adsorptive reactor, the reaction rates (R_{I}, R_{II}, and R_{III}) are faster (10^{-2} to 10^{-3} mol kg^{-1} catalyst s^{-1} for $z = 0$–0.1 m) than that of the adsorption rate (the maximum value is about 10^{-3} mol kg^{-1}adsorbent s^{-1}), the performance of the AER is not evident. But at the left part of the adsorptive reactor (for $z = 0.1$–2 m), the order of magnitude of the reaction rates and the adsorption rate is almost the same. In this case, if the adsorption rate is fast, the reaction rates are fast too, and the performance of the AER is more evident. For example, at $z = 0.5$–1 m, there occurs a peak for the reaction rates at $t = 700$ s (Fig. 5) which corresponds to the peak for the adsorption rate (Fig. 6). Combined with Figs. 3 and 4, the adsorbent is gradually saturated with CO_2 from the inlet part of the adsorptive reactor, the evident AER zone moves toward to the outlet with time, sharp peaks of the AER rates occur at the adsorption front edge where CO_2 is adsorbed at high adsorption rate.

In the adsorptive reactor, the changes of the effectiveness factors are different from those for the conventional reactor. Fig. 7 demonstrates the changes of the effectiveness factor η_j along a 2 m long adsorptive reactor at different times. At the inlet of the adsorptive reactor the reaction rates are fast due to feed of CH_4 and H_2O, there exist the concentration gradients in the catalyst due to the intraparticle-diffusion limitations, as shown in Fig. 8a, where $Z = 0.076$ m; therefore, the effectiveness factors are small. At $t = 100$ s, the

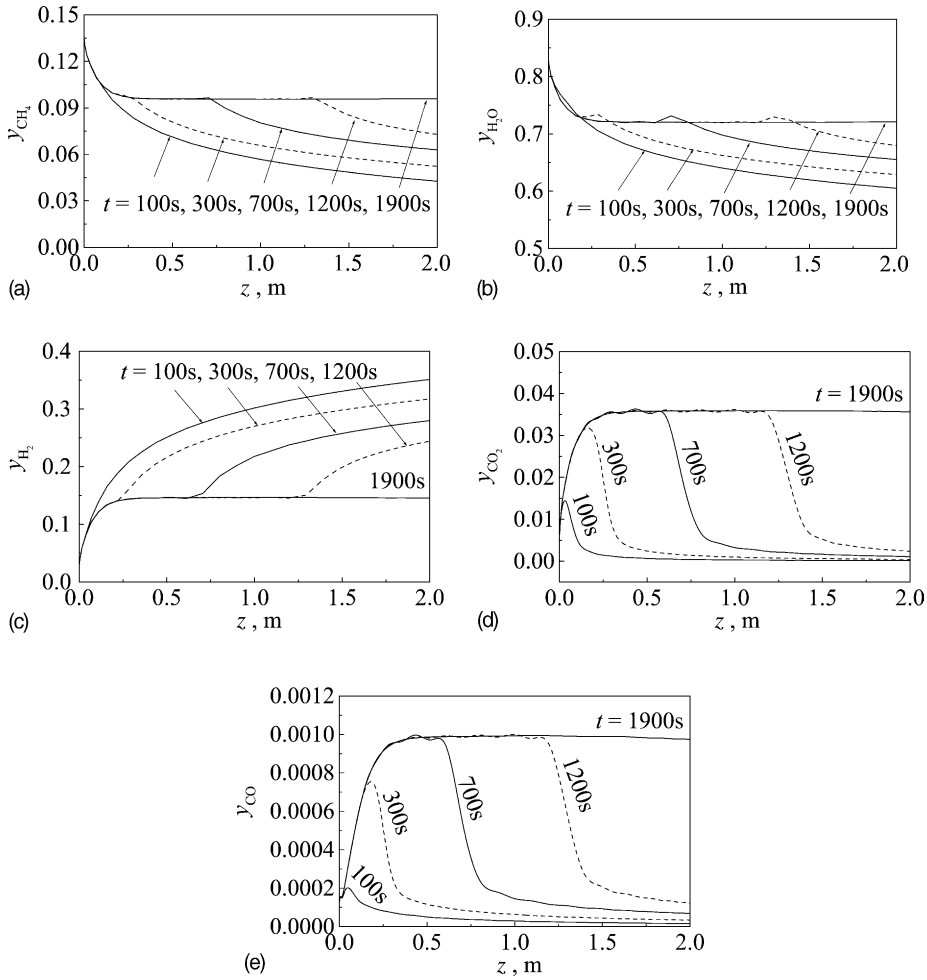

Fig. 4. Mole concentration profiles with time in 2 m adsorptive reactor: (a) CH_4; (b) H_2O; (c) H_2; (d) CO_2; (e) CO. Operation conditions are the same as those in Fig. 1.

adsorbent is not saturated with CO_2 even for the inlet part of the adsorptive reactor, the reaction rates decrease gradually along the adsorptive reactor, then the effectiveness factors correspondingly increase and approach unity at the outlet. At the adsorbent saturated zone, the changes of the effectiveness factors will be similar to those for the conventional reactor. However, at the AER zone, the effectiveness factors vary with the reaction rates due to the intraparticle-diffusion limitations. But the mole concentration gradients in the catalyst pellet are smaller (at $Z = 0.84$ m) than those at the inlet part due to low reaction rates, as shown in Fig. 8b. It should be noted the tendency of η_{III} is different from others when $t = 700$ s, probably because the concentration of CO

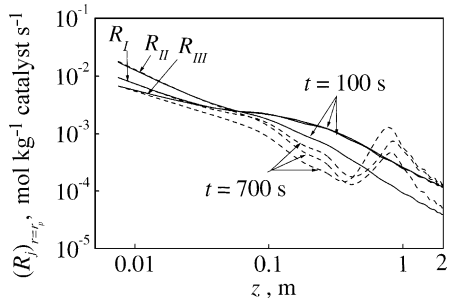

Fig. 5. Reaction rate distributions along with a 2 m length adsorptive reactor at operating times 100 and 700 s.

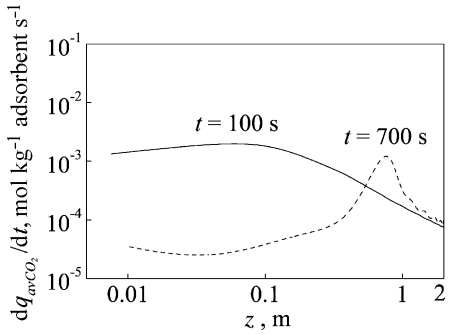

Fig. 6. Adsorption rate distributions along with a 2 m length adsorptive reactor at operating times 100 and 700 s.

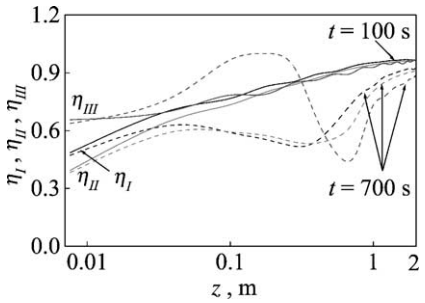

Fig. 7. Effectiveness factors along with a 2 m length adsorptive reactor at operating times 100 and 700 s.

is small, and η_{III} is sensitive to the concentration of CO at this stage.

For many industrial applications, the CO concentration in hydrogen should be controlled (for example, below 30 ppm for fuel cell applications). In other words, the hydrogen purity, the hydrogen productivity and the remaining CO concentration all are important. The purity of hydrogen, the hydrogen productivity and the concentration of CO are sensitive to the conditions such as the length of the adsorptive reactor, the operating temperature and pressure. Table 3 summaries some simulation results (product gas with CO below 30 ppm) to examine the effects of the adsorptive reactor length, the operating temperature and pressure on the hydrogen purity of the product gas and the hydrogen productivity. The adsorption isotherm is taken from paper [9].

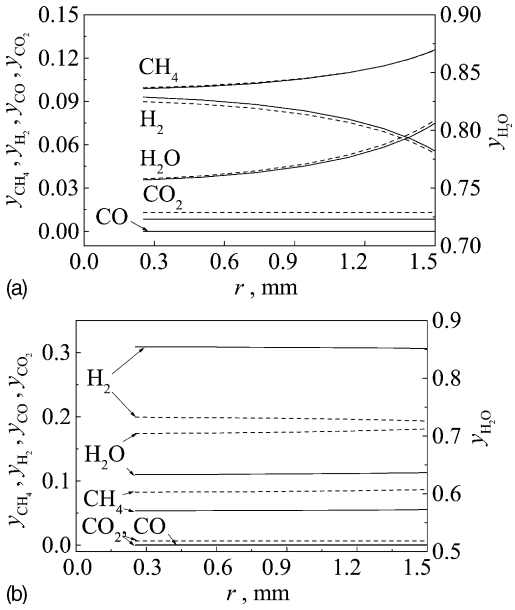

Fig. 8. Mole fraction profiles in 3 mm diameter catalyst pellet at reaction times 100 s (solid lines) and 700 s (dashed lines) in the (a) inlet of the adsorptive reactor ($z = 0.076$ m) and (b) middle of the adsorptive reactor ($z = 0.84$ m).

As shown in runs 1–3, the hydrogen productivity can be effectively improved by increasing the length of the adsorptive reactor due to the increment of adsorbent amount, but there exist some problems in the adsorbent regeneration [10,11]. Low operating temperature effectively decreases

Table 3
Comparison of the simulation results between the Fickian diffusion model (FD model) and LDF($\bar{\eta}_j$) model at various operating conditions

No.	P (kPa)	T (°C)	L (m)	Model (FD and LDF($\bar{\eta}_I$, $\bar{\eta}_{II}$, $\bar{\eta}_{III}$))	Gas quantities (mol kg^{-1} of solid)		Hydrogen product purity (dry)				Methane conversion (%)
					Feed	Hydrogen productivity	H_2 (%)	CH_4 (%)	CO_2 (ppm)	CO (ppm)	
1	445.7	450	2	FD	0.485	0.236	91.9	8.1	302	30	70.1
				LDF(0.78, 0.75, 0.81)		0.229	91.5	8.5	407	38	69.3
2	445.7	450	4	FD	0.614	0.301	92.8	7.2	383	30	73.4
				LDF(0.80, 0.77, 0.81)		0.294	92.2	7.8	415	35	71.6
3	445.7	450	6	FD	0.708	0.344	92.9	7.1	401	30	76.2
				LDF(0.81, 0.78, 0.82)		0.340	92.6	7.4	434	34	73.2
4	445.7	400	4	FD	2.203	0.571	74.9	25.0	1239	30	39.5
				LDF(0.83, 0.80, 0.85)		0.559	74.1	25.8	1301	32	38.2
5	445.7	490	4	FD	0.427	0.265	98.3	1.7	190	30	92.5
				LDF(0.77, 0.75, 0.80)		0.256	97.8	2.2	226	37	90.6
6	222.9	450	4	FD	0.320	0.181	96.7	3.3	288	30	86.5
				LDF(0.75, 0.73, 0.79)		0.178	96.3	3.6	329	37	85.5
7	891.4	450	4	FD	1.528	0.583	86.4	13.6	553	30	58.0
				LDF(0.77, 0.76, 0.79)		0.573	85.7	14.2	609	36	56.5
8	222.9	400	4	FD	0.811	0.283	83.8	16.1	823	30	53.2
				LDF(0.82, 0.79, 0.85)		0.282	83.6	16.3	886	35	52.6
9	891.4	490	4	FD	0.785	0.434	95.4	4.6	259	30	81.4
				LDF(0.74, 0.73, 0.75)		0.423	94.5	5.5	323	40	78.1

$u_f = 0.05$ m s^{-1} for all simulations.

CO concentration in the product gas due to the fact that low temperature is in favor of the adsorption of CO_2 and the exothermic water–gas shift reaction (III). As a result, the hydrogen productivity increases; meanwhile the hydrogen purity in the product gas decreases, as shown in run 4. For example, the hydrogen productivity at 400 °C (run 4) is almost twice of that at 450 °C (run 2), while the hydrogen purity drops from 92.8% (450 °C) to 74.9% (400 °C). Due to reforming reactions (I) and (II) being strongly endothermic, increasing the operating temperature to 490 °C, the hydrogen purity can reach 98.3% for a 4 m long adsorptive reactor (run 5). But the hydrogen productivity will decrease caused by two factors: the adsorption capacity drop and the water–gas shift reaction (reaction (III)) being hindered by higher temperature, with the result that the by-product CO can not be suppressed effectively. In our simulation, the appropriate operating temperature is 450–490 °C.

It is obvious that the low pressure can promote the reforming reactions of (I) and (II) and has no effect on the water–gas shift reaction of (III), whereas the CO_2 adsorption capacity of the adsorbent will drop at low pressure. The effect of the operating pressure on the hydrogen purity and hydrogen productivity is shown in runs 2, 6, and 7. It is found that the hydrogen purity in the product gas increases at lower operating pressure, but the hydrogen productivity decreases greatly. So lower pressure is not a good operating mode. Probably, higher pressure with moderate temperature is an appropriate combination for higher purity hydrogen with high productivity if the adsorption capacity of adsorbent allows, which is well verified by runs 2, 8, and 9.

The accuracy of the model is evaluated by comparing simulation results with the experimental data from Hufton et al. [8] for the single step adsorption-enhanced reaction process. Details of the experiment can be found in literature [8]. According to Hufton et al. [8], the purity of the H_2 product is 96% when the net H_2 productivity is 0.8 mol kg^{-1} (solid). Our simulation results predicts 93% hydrogen product gas with traces of CO (62 ppm) and CO_2 (696 ppm) when the hydrogen productivity is 0.8 mol kg^{-1} of solid, as shown in Fig. 9. Therefore, the simulated results are in reasonable agreement with experimental data from the literature.

The simulation of the cyclic process with the model above involving many components becomes complex and requires high computation time. Therefore, the simulation for the cyclic process (high pressure reaction/adsorption, depressurization, low-pressure purge and pressurization) will be carried out with a simpler model, linear driving force/average effectiveness factor, LDF($\bar{\eta}_j$) applied in our previous work [10,11]. In the LDF($\bar{\eta}_j$) model, the LDF model was adopted to describe the mass-transfer rate of CO_2 inside the adsorbent and the average effectiveness factors, $\bar{\eta}_j$, for the steam-methane reforming reaction in the catalyst pellet are taken over the operating time of the adsorption-enhanced reaction, which can be estimated from the Fickian diffusion model (called FD model) for the catalyst described in this paper. We compare the simulation

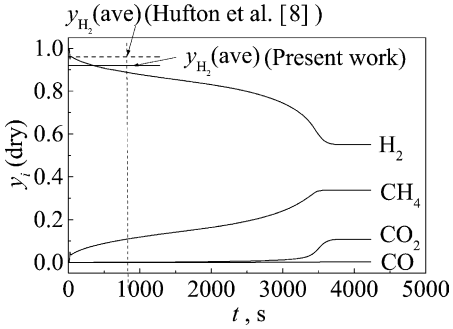

Fig. 9. Effluent mole fraction curves calculated based on the experimental conditions of Hufton et al. [8], where $P_H = 480.3$ kPa, $T_f = T_w = 450$ °C, $L = 1.067$ m, $u_f = 0.031$ m s^{-1}, $H_2O/CH_4 = 6$, $\rho_{cat} = 769$ kg m^{-3}, $\rho_{ad} = 769$ kg m^{-3}, parameters for Langmuir isotherm $m_{CO_2} = 0.85$ mol kg^{-1}, $b_{CO_2} = 3.94 \times 10^{-4}$ Pa^{-1}.

results by LDF($\bar{\eta}_j$) with those by FD model at various operating temperature, operating pressure and length of the adsorptive reactor in Table 3. The simulation results show that the LDF($\bar{\eta}_j$) model can be used to simplify the simulation of the cyclic adsorption-enhanced steam-methane reforming process, but the average effectiveness factors, $\bar{\eta}_j$, should be estimated in advance by an appropriate model like Fickian diffusion model for the catalyst.

4. Conclusions

A theoretical model for the adsorption-enhanced steam-methane reforming is developed, which is a non-isothermal, non-adiabatic, and non-isobaric model and takes into account the effects of intraparticle-diffusion limitations on the reactions and adsorption processes. The simulated results are reasonable compared with experimental data from the literature [8] for single step adsorption-enhanced SMR process. Based on the simulation results, a high purity of hydrogen product gas (90–98%) with traces of CO_2 (below 400 ppm) and CO (below 30 ppm) can be produced directly at 450–490 °C and 222.9–891.4 kPa from an adsorptive reactor due to the adsorbent selectively removing CO_2 from the reaction zone and enhancing the methane conversion.

The mechanism of the adsorption-enhanced SMR is studied by analyzing the profiles of the bed concentrations, temperature, velocity, pressure, reaction and adsorption rates. It is found that the adsorbent is saturated gradually with CO_2 from the inlet part of the adsorptive reactor and spreads to the outlet with time. Correspondingly, the adsorption-enhanced reaction zone moves ahead along the adsorptive reactor and sharp peaks of the AER rates occur at the adsorption front edge. For the adsorption-enhanced SMR process, an evident reaction temperature drop arises due to CO_2 selectively removing and the adsorption-enhanced SMR (reactions (I) and (II)).

The simulated results show that the intraparticle-diffusion limitations should be taken into account in the adsorptive

reactor. The reaction rates are enhanced by adsorption and varied with time in AER zone; the effectiveness factors are difficult to be evaluated compared with conventional reactor. However, the Fickian diffusion model proposed in this paper provides a method to estimate the average effectiveness factor which can then be used in a simpler model (LDF model for adsorbent combined with average effectiveness factors for the catalyst) of the cyclic process to predict the hydrogen purity and productivity, and the concentrations of CO and CO_2 in the product gas for the adsorption-enhanced steam-methane reforming process.

Acknowledgements

One of us (Guohua Xiu) acknowledges financial support from FCT No. SFRH/BPD/1538/2000 and POCTI/32654/EQU/2000. Prof. S. Farooq kindly provided the program for calculating the roots of collocation points and the matrix.

References

[1] S.Z. Roginskii, M.J. Yanovskii, G.A. Graziev, Catalytic reactions and catalysis under chromatographic reactor, Kinetikai Kataliz 3 (1962) 529–540.
[2] C. Chu, L.C. Tsang, Behavior of chromatographic reactor, Ind. Eng. Chem. Proc. Des. Dev. 10 (1971) 47–53.
[3] K. Takeuchi, Y. Uraguchi, Experimental studies of a chromatographic moving bed reactor, J. Chem. Eng. Jpn. 10 (1977) 455–460.
[4] B.K. Cho, R. Aris, R.W. Carr, A continuous chromatographic reactor, Chem. Eng. Sci. 35 (1980) 74–81.
[5] G.G. Vaporciyan, R.H. Kadlec, Equilibrium limited periodic separating reactors, Am. Inst. Chem. Eng. J. 33 (1987) 1334–1343.
[6] G.G. Vaporciyan, R.H. Kadlec, Periodic separating reactors: experiments and theory, Am. Inst. Chem. Eng. J. 35 (1989) 831–844.
[7] Z.P. Lu, A.E. Rodrigues, Pressure swing adsorption reactors: simulation of three-step one-bed process, Am. Inst. Chem. Eng. J. 40 (1994) 1118–1137.
[8] J.R. Hufton, S. Mayorga, S. Sircar, Sorption-enhanced reaction process for hydrogen production, Am. Inst. Chem. Eng. J. 45 (1999) 248–256.
[9] Y. Ding, E. Alpay, Adsorption-enhanced steam-methane reforming, Chem. Eng. Sci. 55 (2000) 3929–3940.
[10] G.H. Xiu, J.L. Soares, P. Li, A.E. Rodrigues, Simulation of five-step one-bed sorption-enhanced reaction process, Am. Inst. Chem. Eng. J. 48 (2002) 2817–2832.
[11] G.H. Xiu, P. Li, A.E. Rodrigues, Sorption-enhanced reaction process with reactive regeneration, Chem. Eng. Sci. 57 (2002b) 3893–3908.
[12] W.E. Waldron, J.R. Hufton, S. Sircar, Production of hydrogen by cyclic sorption enhanced reaction process, Am. Inst. Chem. Eng. J. 47 (2001) 1477–1479.
[13] H.W. Haynes Jr., Multicomponent diffusion and reaction in porous catalysts, in: M.P. Dudukovic, P.L. Mills (Eds.), ACS Symposium Series 237, Chemical and Catalytic Reactor Modeling, American Chemical Society, Washington, DC, 1984.
[14] J. Skrzypek, M. Grzesik, R. Szopa, Theoretical analysis of two parallel and consecutive reactions in isothermal symmetrical catalyst pellets using the dusty-gas model, Chem. Eng. Sci. 39 (1984) 515–521.
[15] G.H. Graaf, H. Scholtens, E.J. Stamhuis, A.A.C.M. Beenackers, Intra-particle diffusion limitations in low-pressure methanol synthesis, Chem. Eng. Sci. 45 (1990) 773–783.
[16] F.H. Hartig, F.J. Keil, Large-scale spherical fixed-bed reactors: modeling and optimization, Ind. Eng. Chem. Res. 32 (1993) 424–437.
[17] S.S.E.H. Elnashaie, S.S. Elshishini, Modelling, Simulation and Optimization of Industrial Fixed Bed Catalytic Reactors, Gordon and Breach, Amsterdam, 1993.
[18] T.S. Pan, B.C. Zhu, Study on diffusion-reaction process inside a cylindrical catalyst pellet, Chem. Eng. Sci. 53 (1998) 933–946.
[19] S. Ergun, Fluid flow through packed columns, Chem. Eng. Prog. 48 (1952) 89–94.
[20] J. Xu, G.F. Froment, Methane steam reforming, methanation and water–gas shift. 1. Intrinsic kinetics, Am. Inst. Chem. Eng. J. 35 (1989) 89–96.
[21] M.V. Twigg, Catalyst Handbook, Wolfe Publishing Ltd., UK, 1989.
[22] A. Malek, S. Farooq, Study of a six-bed pressure swing adsorption process, Am. Inst. Chem. Eng. J. 43 (1997) 2509–2523.
[23] M.F. Edwards, J.F. Richardson, Gas dispersion in packed beds, Chem. Eng. Sci. 23 (1968) 109–123.
[24] S. Yagi, D. Kunii, N. Wakao, Studies on axial effective thermal conductivities in packed beds, Am. Inst. Chem. Eng. J. 6 (1960) 543–546.
[25] A.P. De Wash, G.F. Froment, Heat transfer in packed bed, Chem. Eng. Sci. 27 (1972) 567–576.
[26] C.H. Li, B.A. Finlayson, Heat transfer in packed bed—a reevaluation, Chem. Eng. Sci. 32 (1977) 1055–1066.
[27] N. Wakao, T. Funazkri, Effect of fluid dispersion coefficients on particle-to-fluid mass transfer coefficients in packed beds, Chem. Eng. Sci. 50 (1978) 2507–2552.
[28] Y. Ding, E. Alpay, Equilibria and kinetics of CO_2 adsorption on hydrotalcite adsorbent, Chem. Eng. Sci. 55 (2000) 3461–3474.
[29] R. Wang, S. Farooq, C. Tien, Maxwell–Stefan theory for macropore molecular-diffusion-controlled fixed-bed adsorption, Chem. Eng. Sci. 54 (1999) 4089–4098.
[30] R.C. Reid, J.M. Prausnitz, T.K. Sherwood, The Properties of Gases and Liquids, McGraw-Hill, New York, 1977.
[31] R. Taylor, R. Krishna, Multicomponent Mass Transfer, Wiley, New York, 1993.
[32] R.B. Bird, W.E. Stewart, E.N. Lightfoot, Transport Phenomena, Wiley, New York, 1960.